Design and Implementation of a High Precision Stewart Platform for a Space Camera

Design and Implementation of a High Precision Stewart Platform for a Space Camera

Fengchao Liang*, Shuang Tan, Jiankai Fan, Zhe Lin and Xiaojun Kang

Beijing Institute of Space Mechanics & Electricity, Beijing 100094, China
Email: fc.liang@qq.com

Abstract. In order to design and implement a high-precision Stewart platform to precisely adjust the position and posture of the secondary mirror of a space camera, the following measures were taken: firstly, the inverse mathematical model and ADAMS parametric model of the Stewart platform are established, which are the basis of structural optimization design; secondly, the structural parameters of Stewart platform are obtained through structure optimization design in ADAMS after determining the objective function; thirdly, a 50nm resolution driving strut based on brushless DC motor, ball screw, grating ruler and PI closed-loop control law is designed, which strongly guaranteed the six degrees' resolution of the Stewart platform that mainly consist of 6 such high-resolution driving struts; finally, the accuracy of Stewart platform is tested via dual frequency laser interferometer and photoelectric autocollimator, and the test results show that the displacement resolution of the Stewart platform is 0.2 μ m, and the angular resolution is 1", which meets the requirements of the index. The Stewart platform has been successfully applied to the space camera by tuning the secondary mirror precisely in 6 degrees of freedom in the optical alignment experiment, which lays a solid theoretical and practical foundation for on orbit application in future.
Keywords. 6 DOF, Stewart platform, space camera, parallel mechanism.

1. Introduction

With the continuous improvement of the resolution requirement of space optical camera, ultra long focal length and ultra large aperture space optical remote sensor has become one of the important research directions in the field of earth observation. According to the Rayleigh criterion, the larger the aperture is, the higher the diffraction limit resolution is when the orbit height and the observation spectrum are fixed. In order to achieve sub meter level ground sampling distance on 500 km orbit, the aperture of space camera is required to be 3 meters, while the aperture of space camera is required to be more than 8 meters to achieve meter level optical observation in geostationary orbit. However, due to the limitation of the mirror processing ability and the size of the fairing of the launch vehicle, the primary mirror of the large aperture and high-resolution space telescope usually adopts the block deployable design. Due to the limited accuracy of the deployment mechanism of the primary mirror, there will be multi degree of freedom pose errors in each segmented mirror of the primary mirror. At the same time, with the increase of the focal length of the optical system and the distance between the primary and secondary mirrors, the distance between the primary and secondary mirrors and the spatial pose of the secondary mirror will inevitably change due to the change of the force and thermal environment after the camera enters the orbit. So, the multi degree of freedom adjustment mechanism connected behind the segmented mirror and secondary mirror must implement on orbit correction to meet the requirements of high-resolution imaging of space telescope.

The existing 6-DOF pose adjustment schemes mainly include series mechanism and parallel mechanism. Compared with the traditional series mechanism, Stewart parallel mechanism has the advantages of high precision, high stiffness, high stability, small error, small friction and good dynamic performance [1, 2]. Parallel mechanism is suitable for high precision and large load. The high-precision 6-DOF parallel platform is one of the key actuators to realize on orbit adaptive optics of space optical remote sensor. For instance, Stewart parallel mechanism is used in the blocked primary mirror and secondary mirror of James Webb Space Telescope [3, 4], and is used in the secondary mirror adjustment of Herschel Space Telescope developed and launched by ESA [5] in 2009 and is also used in VST launched in Italy in 2012 [6].

In our space camera project, there is an urgent need to develop a high-precision 6-DOF platform to adjust the position and pose of the secondary mirror precisely, so as to realize the optical alignment of the ground state. The aperture of the secondary mirror is about 0.5 m and the weight is about 25 kg. The main indexes of the platform are as follows: X / Y / Z translation range is ± 2 mm with 0.2 μm resolution, angle range that rotating around X / Y / Z is ± 1 °with 1" resolution, and the carrying capacity is 25 kg. The main process of design and implementation such a high precision 6-DOF platform is given below.

2. Kinematic Analysis

The kinematics analysis of parallel mechanism is the basis of dynamics analysis, control strategy research and structure optimization design, so it is very important to establish an accurate kinematics model for the research of parallel mechanism. The structure of a Stewart parallel mechanism is shown in figure 1 [7, 8], which is composed of two platforms and six parallel, independent and freely retractable driving struts. The driving struts and the platforms are connected by Hooke hinges A_1, A_2, A_3, A_4, A_5, A_6 and Hooke hinges B_1, B_2, B_3, B_4, B_5, and B6. The lower platform is used as the static platform, and the displacement of the driving strut is used as the input variable to control the spatial displacement and posture of the moving platform (upper platform). The 6-DOF movement of the moving platform, the translation along the X, Y, Z axes and the Euler angles U, V, W around the X, Y, and Z axes, is realized by changing the length of six retractable driving struts.

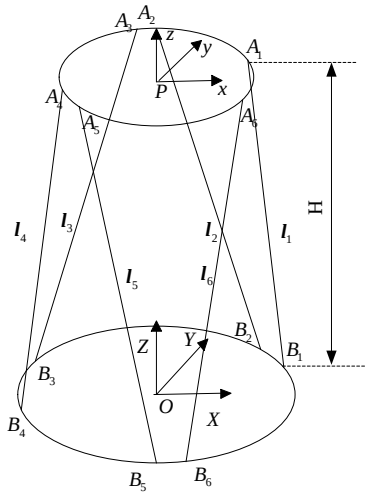

Figure 1. Coordinate systems of 6-DOF Stewart Platform.

In order to quantitatively represent the coordinates of the moving platform, the static coordinate system *O-XYZ* is established at the center of the circle where the hinge points of the static platform are located, the dynamic coordinate system *P-xyz* is established at the center of the circle where the hinge points of the moving platform is located. The origins of the coordinates are *O* and *P* separately, and the direction of each coordinate system is shown in figure 1. After the coordinate system is determined,

the pose of the moving platform is expressed by the generalized coordinate vector $\boldsymbol{q}$, where $\boldsymbol{q} = [q_1, q_2, q_3, q_4, q_5, q_6]^T$, $[q_1, q_2, q_3]^T$ and $[q_4, q_5, q_6]^T$ represent the coordinate vector and the attitude angle of the moving coordinate system in the static coordinate system, separately. These six parameters determine the spatial pose of the moving platform. In this paper, the finite rotation of a rigid body about an axis mentioned in Euler's theorem is decomposed into three finite rotations around the coordinate axis of the connected body in a certain order, and the angle of each rotation can be defined as three generalized coordinates to determine the relative position of the rigid body before and after rotation. According to the different rotation order, there are 24 rotation ways. We choose the rotation order of rounding $z \rightarrow y \rightarrow x$ axis of the moving coordinate system in turn, which is the same as the result of three times of rotation around the fixed axis of the static coordinate system in reverse order [9, 10]. After three rotations, the final rotation transformation matrix can be obtained as shown in equation (1)

$$ {}^{O}_{P}\mathbf{R} = \mathbf{R}(z,W)\cdot\mathbf{R}(y,V)\cdot\mathbf{R}(x,U) = \begin{bmatrix} cWcU & cWsVsU - sWcU & cWsVcU + sWsU \\ sWcV & sWsVsU + cWcU & sWsVcU - cWsU \\ -sV & cVsU & cVcU \end{bmatrix} \tag{1} $$

where *cU = cos (U), cV = cos (V), cW = cos (W), sU= sin (U), sV = sin (V), sW = sin (W).* When the generalized coordinate system $\boldsymbol{q} = [X, Y, Z, U, V, W]^T$, the length of each driving strut is shown in equation (2)

$$ l_i = \left|l_i\right| = \sqrt{l_i^T \cdot l_i} \tag{2} $$

where $\boldsymbol{l_i}$ is the driving struts' vector $\boldsymbol{A_iB_i}$ shown in figure 1, and l_i is the driving strut length, i = 1, 2,..., 6. So far, the inverse kinematics equation of Stewart Parallel mechanism is established.

3. Structural Optimization Design

The selection of structural parameters of 6-DOF parallel mechanism directly affects the kinematic performance of the mechanism. The optimal design of parallel mechanism is to find a group of optimal parameters to make the parallel mechanism have better performance.

3.1. Parametric Modeling

ADAMS provides the function of parametric modeling, that is, the eigenvalues of the model are expressed by the design parameters in ADAMS, so that the model will change automatically with the modification of the design parameters. In particular, when making parameter analysis in ADAMS, the design parameters are averaged in the set range, the model is automatically updated, and ADAMS automatically carries out a series of simulation, which can observe the performance of the prototype under different parameter values.

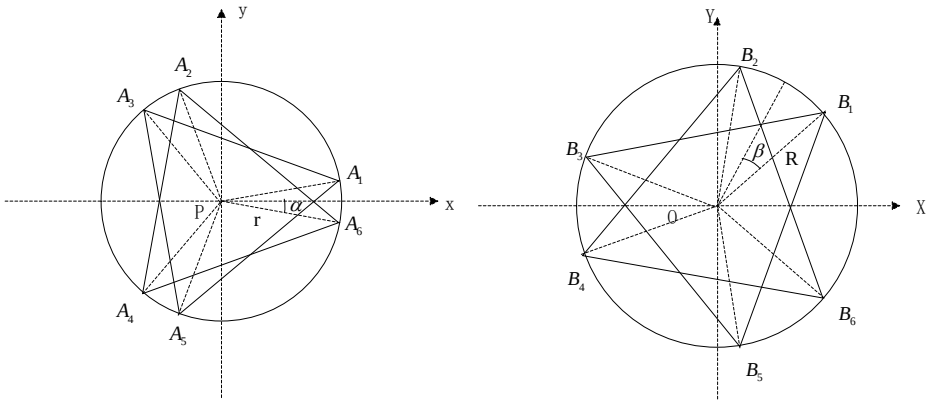

Figure 2. Location distribution of hinge points of moving platform and static platform.

As shown in figure 1 and figure 2, the Stewart platform is simplified as a static platform, a moving platform, six driving struts, six upper Hook hinges and six lower Hook hinges. The structure parameters of the Stewart platform are *r*, *R*, α**,** *β* and *H***.** The basic structure of Stewart platform can be fully described by the five parameters above. In ADAMS parameterization, *r*, *R*, α**,** *β* and *H* are parameterized into *rtop*, *topalpha*, *rbottom*, *bottombeta* and *H*, respectively. The parametric model is shown in figure 3.

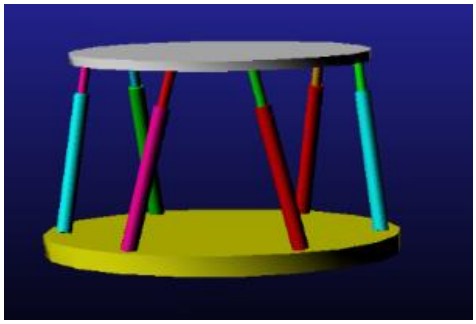

Figure 3. Parametric model of the Stewart platform.

3.2. Establishment of Objective Function and Constraint Equation

In the design of Stewart platform, the change of the displacement of the driving strut is the most intuitive variable. Given the same motion index, the shorter the stroke of the driving strut is, the smaller the driving speed and the smaller the energy loss is. The smaller the stroke of the driving strut is, the shorter the movement time and the better the stiffness of the mechanism is. The larger the stroke of the driving strut is, the higher the probability of singularity configuration is. Therefore, the optimal objective function is to minimize the absolute value of the expansion and contraction of the six driving struts in the motion

$$f(x)=\min\left(\max\left(\max\left|L_i(x)-L_i(0)\right|\right)\right) \tag{3}$$

x is an independent variable, which is determined by the design variables *r*, *R*, *α***,** *β* and *H*, *x* = [*r R α β H*], L_i *(0)* is the length of the i^{th} driving strut when the parallel platform is at zero position, and L_i *(x)* is the length of the i^{th} driving strut of the moving platform, then the increment of the i^{th} driving strut *DL* = L_i *(x)* - L_i *(0)*. After determining the objective function, we need to determine the constraints of the function.

3.2.1. Radius Constraints of Platforms and Driving Struts. For the general parallel mechanism, the static platform usually has a larger parameter value than the moving platform. So the constraint equation of the platform is r – R ≤0. The minimum value of distribution angle of moving and static platform α and β are related to the radius parameter of the driving struts. If the parameter is improper, it will cause mechanical interference between the driving struts. Therefore, it is necessary to establish constraints. Considering 20% margin, the constraint equations are as equation (4).

$$\begin{cases} r-R<0 \\ 1.2arc\sin(\dfrac{r\_strut\_up}{r})-\alpha\le 0 \\ 1.2arc\sin\left(\dfrac{r\_strut\_bottom}{R}\right)-\beta\le 0 \end{cases} \tag{4}$$

In equation (4), *r_strut_up* is the radius of the moving rod of the driving strut, and *r_strut_bottom* is the radius of the static rod of the driving strut.

3.2.2. Length Constraint of Driving Strut. This is to set the maximum travel of the driving strut in the workspace. The working space of the secondary mirror platform is relatively small, ±2mm and ±1 °, so the stroke of the driving strut is small. Considering the space limitation of the mechanism in the motion, according to the preliminary design results of the single driving strut, the median length of the driving strut is not less than 272.3mm, and the length range is [260, 290] mm. Therefore, the constraint equation of the length of the driving strut is

$$\begin{cases} 260-\min\left(L_i\right)\le 0 \\ \max\left(L_i\right)-290\le 0 \\ L_0\ge 272.3 \end{cases} \tag{5}$$

3.2.3. Upper and Lower Hinge Angle Range Constraint. Due to the limitation of the rotation angle range of the actual Hooke hinge, the rotation angle of the Hooke hinge designed in the parallel mechanism is greater than 3 °. Reserve part of the margin, set the constraint angle to 5 °, so the constraint equation of Hooke hinge angle range is

$$\begin{cases} \max\left(\left(\gamma_d\right)_i\right)-5^\circ\le 0 \\ \max\left(\left(\gamma_u\right)_i\right)-5^\circ\le 0 \end{cases} \tag{6}$$

To sum up, in the structural optimization design of the Stewart platform, it is to find a set of structural parameters $x = [r\ R\ \alpha\ \beta\ H]$ to satisfy equation (7).

$$\begin{cases} \min \quad f\left(x\right)=\max\left(\max\left|L_i\left(x\right)-L_i\left(0\right)\right|\right) \\ s.t. \quad \begin{array}{c} 227\le r\le 244 \\ 227\le R\le 249 \\ 195\le H \\ \dfrac{r_{strut\_top}}{r}<\sin\left(\alpha\right)<\dfrac{\pi}{6} \\ \dfrac{r_{strut\_bottom}}{R}<\sin\left(\beta\right)<\dfrac{\pi}{6} \\ L_0\ge 272.3 \\ r-R\le 0 \\ L_{\min}-\min\left(L_i\right)\le 0 \\ \max\left(L_i\right)-L_{\max}\le 0\le 0 \\ \max\left(\left(\gamma_d\right)_i\right)-5^\circ\le 0 \\ \max\left(\left(\gamma_u\right)_i\right)-5^\circ\le 0 \end{array} \end{cases} \tag{7}$$

where L_0 is the median length of the driving strut, and the expression is

$$L_0=\sqrt{H^2+\left[\left({}^{P}A_{1x}-B_{1x}\right)^2+\left({}^{P}A_{1y}-B_{1y}\right)^2\right]} \tag{8}$$

According to equation (7), the objective function and constraint equation are established in ADAMS to optimize the structure.

3.3. Results of Structural Optimization Design

The structure optimization of the Stewart platform includes three steps: design research, experimental design and optimization design. Design research is to study the influence of the five design parameters of the Stewart platform on the performance of the mechanism. Experimental design is to study the changes of multiple design variables, and to group the values of multiple design variables to study the value of objective function when the design variables take different possible combinations. Experimental design is the design research in ADAMS, and only a single design variable change. Optimal design is to find a group of structural parameters x, which satisfy the constraint condition equation (7). After several times of optimization, the final optimization results are: r = 239.51mm, R = 249mm, H = 195.03mm, α= 0.115rad, β= 0.134rad.

4. Stewart Platform Design

4.1. Resolution Requirements of Driving Strut

The resolution of Stewart platform mainly depends on the resolution of each driving strut. In practical engineering, the resolution of each driving strut is limited, which will cause the resolution of the platform to be limited, too. Therefore, the inverse solution of the displacement resolution of the driving strut should be calculated to obtain the required resolution of the driving strut. According to the resolution requirement of the Stewart platform, 0.2 μm and 1", a driving strut with at least 60 nm motion resolutions should be designed and realized first.

4.2. Torque Demand of Driving Strut

The mass of the Stewart platform is 26.74 kg, in which the mass of the moving platform is 3.95 kg. So the actual total load of the Stewart platform is 28.95 kg, including the mass of the moving platform and the secondary mirror. Through ADAMS simulation, the force situation of six driving strut is shown in figure 4, and the maximum value is 108.8 N. Therefore, in the ground working state, the driving strut should provide at least 108.8 N driving force. After calculation, the DC servo motor with continuous locked rotor torque of 0.706 NM is selected, which has a torque margin of 6.67 to meet the load capacity and instantaneous overload requirements of the secondary mirror platform.

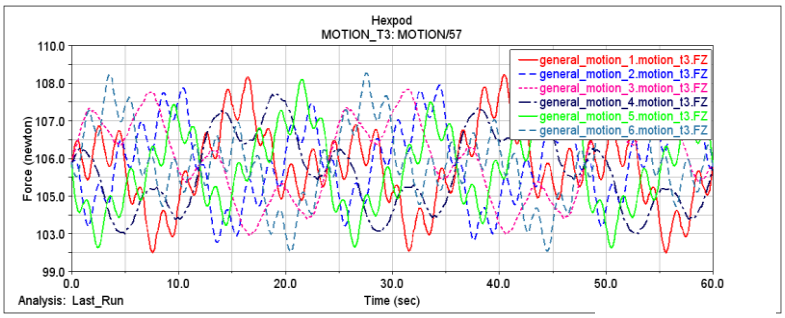

Figure 4. Force curves of six driving struts.

4.3. High Resolution Driving Strut Design

Because the pose adjustment of the 6-DOF Stewart platform is realized by controlling stretch of six driving struts precisely, the high resolution driving struts are core components of the platform. To design such a high precision 6-DOF Stewart platform, one of the key and difficult techniques is how to realize the high-resolution drive strut. With the improvement of ball screw assembly technology, the servo drive mechanism of DC servo motor and ball screw has higher and higher stiffness and precision. This design adopts the driving mechanism of "DC servo motor + ball screw + grating ruler feedback". As shown in figure 5, the driving strut is composed of hook hinge, power transmission part of lead screw guide rail, closed-loop feedback part of absolute grating ruler and in place locking part. The

screw is directly driven by DC servo motor, and the screw nut moves along the length of the strut under the passive constraint of the moving platform. In order to eliminate the influence of the passive rotation of the driving strut around the rod on the moving distance of the lead screw, a 5 nm resolution grating ruler is used to measure the moving distance directly, and closed-loop servo control of eliminating static error is used too. As a result, the resolution of the driving strut reaches to 50 nm, better than 60 nm. Figure 5 also shows the 50 nm displacement step response curve of the driving strut.

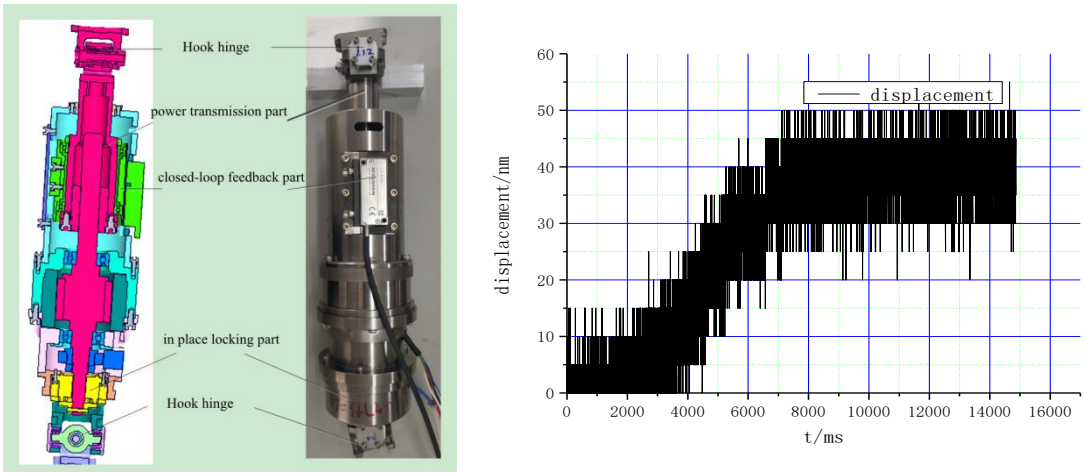

Figure 5. Driving strut with 50 nm displacement resolution.

When the displacement resolution of the driving strut is 50 nm, the resolution of the Stewart platform can be obtained by forward kinematics analysis. The analysis results show that the resolution of 6-DOF Stewart platform are X 0.14μm, Y 0.08μm, Z 0.07μm, U 0.109″, V 0.114″and W 0.066″. It can be seen that the translation resolution is better than 0.2 μm, and the angular resolution is better than 1".

5. Platform Resolution

The Stewart platform is shown in figure 6. The 6-DOF resolution is the key to realize the precise adjustment of the secondary mirror pose. To test the resolution index of this platform, a six degree of freedom pose measurement system was established. The system consists of Renishaw XL-80 dual frequency laser interferometer, automatic collimator, Stewart platform, secondary mirror and parallel mechanism controller. The dual frequency laser interferometer is used to measure the translation resolution, and the collimator is used to measure the rotation resolution. The whole test system is built on the vibration isolation optical platform in the constant temperature laboratory, which can effectively prevent the deformation error caused by temperature drift, isolate and attenuate the low-frequency and high-frequency vibration.

Figure 6. The 6-DOF Stewart platform.

The resolution test of the platform adopts the method of testing each degree of freedom separately. Each degree of freedom is first stepped by 5 times of the technical requirements, and stays for about 20s, so as to make the equipment fully stable, then step forward, and then step backward. Then follow this step to gradually reduce the command value, such as X direction resolution test, respectively X translation 1 μm, 0.8 μm, 0.6 μm, 0.4 μm, 0.2 μm, 0.1 μm. The laser interferometer test curve can well distinguish X translation 1 μm to 0.2 μm, and continue to try to give a smaller translation instruction of 0.1 μm. The step of displacement curve is not obvious, so the resolution of X translational degree of freedom is 0.2 μm. Similarly, the translation resolution of Y and Z degrees of freedom is 0.2 μm, and the resolution of the platform rotating around X, Y and Z axis is 1″. The experimental results show that the X, Y, Z translation resolution of the Stewart platform is 0.2 μm, and the resolution of rotation around X, Y and Z is 1 ", which meets the requirements of the index.

6. Conclusion

In view of two outstanding difficulties, the structural optimization design and the high resolution driving strut design, in the development of high-precision Stewart platform, this paper gives the following design and implementation methods:

1) Based on the mathematical model and parametric model of the 6-DOF Stewart platform, the objective function of minimum elongation of the driving strut is determined. Combined with the constraints of the strut length and hinge angle, the structural optimization design is completed, and the Stewart platform structure meeting the requirements of multi index is obtained.

2) According to the requirement of high resolution driving strut, the driving strut based on "DC servo motor + ball screw + grating ruler" is designed, and the strut's resolution reaches to 50 nm, which is one of the powerful guarantees for the high resolution of the Stewart platform.

The optical test results show that the resolution of Stewart platform is 0.2 μm. The resolution of rotation angle is 1 ", which meets the requirements of ground optical alignment and on orbit active optical adjustment of the space camera.

Acknowledgments

I would like to thank all colleagues who have helped in this research work, such as Dr. Yu Fei, deputy director Kang Jianbing, etc.

References

[1] Merlet J P 2006 *Parallel Robots* 2nd (Netherland: Springer Science & Business Media) pp 66-74.
[2] Kong X W 2008 *Type Synthesis of Parallel Mechanisms* Springer Berlin Heidelberg pp 1-4.
[3] Clampin M 2011 The James Webb Space Telescope (JWST) *Advances in Space Research* **41** 1983–1991.
[4] Warden R M 2006 Cryogenic Nano-Actuator for JWST *Proceedings of the 38th Aerospace Mechanisms Symposium* p 239-252.
[5] Toulemont Y, Passvogel T, et al. 2004 The 3.5m all SiC telescope for HERSCHEL *Optical, Infrared, and Millimeter Space Telescopes* 1119-1128.
[6] Schipani P, Perrotta F, Molfese C, et al. 2008 The VST secondary mirror support system *Advanced Optical and Mechanical Technologies in Telescopes and Instrumentation* **28** 1-10.
[7] Gough V E and Whitehall S G 1962 Universal Tyre Test Machine *Proceedings of the 9th International Technical Congress* (London: Institution of Mechanical Engineers) p 117-137.
[8] Stewart D 1965 A platform with six degrees of freedom *Proceedings of International Mechanical. Engineering* **180**(15) 370-386.
[9] Huang Z, Kong L F and Fang Y F 1997 *Mechanism Theory and Control of Parallel Manipulator* (Beijing: China Machine Press) pp 18-29.
[10] Craig J J 2005 *Introduction to Robotics Mechanics and Control* Prentice Hall pp 28-41.